Accepted Manuscript

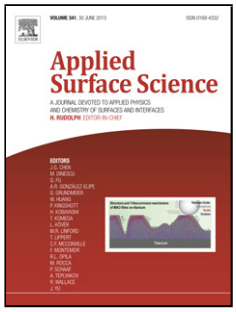

Title: Superhydrophobic aluminum alloy surfaces prepared by chemical etching process and their corrosion resistance properties

Author: Ying Huang D.K. Sarkar X. Grant Chen

PII: S0169-4332(15)01979-0
DOI: http://dx.doi.org/doi:10.1016/j.apsusc.2015.08.166
Reference: APSUSC 31113

To appear in: *APSUSC*

Received date: 5-6-2015
Revised date: 29-7-2015
Accepted date: 19-8-2015

Please cite this article as: Y. Huang, D.K. Sarkar, X.-G. Chen, Superhydrophobic aluminum alloy surfaces prepared by chemical etching process and their corrosion resistance properties, *Applied Surface Science* (2015), http://dx.doi.org/10.1016/j.apsusc.2015.08.166

This is a PDF file of an unedited manuscript that has been accepted for publication. As a service to our customers we are providing this early version of the manuscript. The manuscript will undergo copyediting, typesetting, and review of the resulting proof before it is published in its final form. Please note that during the production process errors may be discovered which could affect the content, and all legal disclaimers that apply to the journal pertain.

ACCEPTED MANUSCRIPT

Superhydrophobic aluminum alloy surfaces prepared by chemical etching process and their corrosion resistance properties

Ying Huang, D. K. Sarkar[*]*, X-Grant Chen*

Centre Universitaire de Recherche sur l'Aluminium (CURAL), Université du Québec à Chicoutimi, 555 Boulevard de l'Université, Chicoutimi, Québec, Canada G7H 2B1

CORRESPONDING AUTHOR'S EMAIL:[*]dsarkar@uqac.ca

CORRESPONDING AUTHOR'S TELEPHONE: 1 (418) 5455011 Ext. 2543

Highlights

1. Fabrication of superhydrophobic aluminum alloy surfaces by chemical etching followed by organic molecule passivation.
2. The formation of flake-like micro-nanostructure morphology of the low surface energy aluminum stearate on aluminum
3. The complementary corrosion studies by polarization resistance and electrochemical impedance spectroscopy (EIS)
4. The modulus of impedanceis found be 70 times larger for the superhydrophobic surfaces compared to the as-received aluminum alloy surface

Accepted Manuscript

ACCEPTED MANUSCRIPT

ABSTRACT

Superhydrophobic aluminum alloy surfaces are obtained by chemical etching using 1 M NaOH solution followed by passivation using 0.01 M ethanolic stearic acid (SA) solution. The formation of low surface energy aluminum stearate takes place during the passivation process between stearic acid and hydroxyl group terminated aluminum alloy surfaces. A schematic model of the SA passivation process on the –OH terminated Al-surfaces is presented in this work. The flake-like micro-nanostructure morphology of the low surface energy aluminum stearate increases the water contact angle by more than 150°, demonstrating the superhydrophobic properties. The corrosion current density reduces and polarization resistance increase systematically with increasing passivation time. The polarization resistance, calculated from the Tafel curve of the superhydrophobic surfaces prepared by stearic acid passivation for 60 min, is determined to be 137 times larger than that of the as-received aluminum alloy substrate. Similarly, the modulus of impedance, as determined from electrochemical impedance spectroscopy (EIS), is found be 70 times larger for the superhydrophobic surfaces compared to the as-received aluminum alloy surface. These results demonstrate that the superhydrophobic aluminum alloy surfaces created by chemical etching followed by passivation have superior corrosion resistance properties than the as-receive aluminum alloy substrate.

Keywords: Corrosion resistance, Superhydrophobic aluminum alloy surfaces, Chemical etching,

Accepted Manuscript

ACCEPTED MANUSCRIPT

Aluminum stearate, Potentiodynamic polarization, Electrochemical impedance spectroscopy (EIS)

1. Introduction

Superhydrophobicity is the property that describes the non-wetting characteristics of material surfaces. Superhydrophobic surfaces are attracting ever increasing attention from the scientists and engineers due to wide applications in corrosion resistance and anti-sticking of snow and ice and potential incorporation into eyeglasses, windows, self-cleaning automobile windshields, and other technologies [1-3]. Recently, various fabrication methods for superhydrophobic surfaces have been explored [4-16]. These methods are guided by the common principles of optimizing topography and lowering surface energy. In other words, both the surface geometrical structure and the chemical composition control the wettability of the solid surface.

Chemical etching process is the process of removing a layer on a metal surface through a chemical reaction and is an effective method for obtaining rough surfaces. It has been widely used to fabricate superhydrophobic aluminum alloy surfaces [6, 7, 17-21]. Sarkar *et al.* obtained superhydrophobic aluminum surfaces by chemical etching followed by coating with an ultrathin rf-sputtered Teflon film [14]. Saleema *et al.* used a one-step etching process to obtain a superhydrophobic aluminum alloy substrate with a NaOH and fluoroalkylsilane (FAS-17) mixed solution [6, 7]. Ruan *et al.* utilized HCl mixed with HF as an etchant on an aluminum alloy substrate followed by passivation with different modifiers such as dodecyl mercaptan (DDM), lauric acid, myristic acid and palmitic acid [17]. Similarly，HCl was also used by Escobar *et al.*

Accepted Manuscript

ACCEPTED MANUSCRIPT

in a chemical etching process, together with passivation employing dodecanoic acid, to obtain superhydrophobic aluminum alloy substrates [18]. In addition, Liao *et al.* fabricated superhydrophobic aluminum alloy substrates by copper assisted chemical etching with HCl solution followed by passivation with hexadecyltrimethoxysilane [19].

A number of investigations have been performed on other superhydrophobic surfaces (apart from aluminum alloy substrates) obtained by chemical etching, such as superhydrophobic silicon etched by HF mixed with $AgNO_3$ followed by passivation with trimethoxysilane [22], superhydrophobic titanium etched by NaCl followed by passivation with tridecafluoroctyltriethoxysilane [23], superhydrophobic zinc (Zn) etched by $NaCl/NaNO_3$ followed by passivation with fluorinated polymer [24], superhydrophobic magnesium etched by H_2SO_4/H_2O_2 followed by passivation with stearic acid (SA) [25] and superhydrophobic copper etched by HNO_3 followed by passivation with 1H,1H,2H,2H-perfluorodecyltriethoxysilane (FDTES) [26].

It is well known that the contact of metals with water triggers corrosion; therefore, one may consider using superhydrophobic surfaces to repel water and thus prevent corrosion. The corrosion resistance properties of superhydrophobic aluminum alloy substrates have been studied in the literature [3, 27-29]. He *et al.* investigated the corrosion resistance of superhydrophobic aluminum alloy substrates, prepared by anodizing followed by passivation with myristic acid, via potentiodynamic polarization experiments as well as electrochemical impedance spectroscopy (EIS) [3]. A similar method for preparing superhydrophobic aluminum alloy substrates has also been used by Liu *et al.*, and the reduced microbiologically influenced corrosion of superhydrophobic

Accepted Manuscript

ACCEPTED MANUSCRIPT

aluminum alloy substrates was investigated using EIS, polarization as well as scanning electron microscopy (SEM) [28]. Furthermore, Liang *et al.* developed a facile sol–gel method, with tetraethylorthosilicate (TEOS) and vinyltriethoxysilane (VTES) as co-precursors at room temperature, to create a superhydrophobic aluminum alloy substrate [27], the authors then characterized the corrosion resistance and durability of the superhydrophobic silica-based surface formed on the aluminum substrate in a corrosive NaCl solution via EIS measurements [27]. In another study by Liu *et al.* [29], the corrosion resistance properties of a superhydrophobic aluminum alloy substrate, fabricated by graphene spin-coated on the surface, were investigated and compared with those of the as-received aluminum alloy substrate.

In our previous study, superhydrophobic copper surfaces were fabricated by a one-step electrochemical modification process with ethanolic stearic acid solution using a DC voltage [13]. Furthermore, the corrosion resistance of the superhydrophobic copper substrates was investigated by potentiodynamic polarization experiments [30]. The decrease of corrosion current density (I_{corr}) as well as the increase of polarization resistance (R_p) obtained from the polarization curves revealed that the superhydrophobic film on the copper surfaces improved the corrosion resistance of the copper substrate. In a recent study from our group, anti-corrosion and anti-icing superhydrophobic steel coatings were achieved by electrodeposition of Zn on steel followed by functionalization of Zn using an ultra-thin film of commercial silicone polymer [31].

In the present study, superhydrophobic aluminum alloy substrates were prepared by chemical etching using alkaline NaOH solution followed by passivation with ethanolic stearic acid (SA) solution. Chemical etching has the technological advantages of being both cost-effective and easy to

Accepted Manuscript

ACCEPTED MANUSCRIPT

scale up. The fabricated superhydrophobic aluminum alloy substrates were analyzed using both potentiodynamic polarization and electrochemical impedance spectroscopy (EIS) to evaluate their corrosion properties.

2. Experiments

As starting materials, rolled sheets of AA 6061 aluminum alloy were chemically etched using 1 M alkaline NaOH solution (pH of 14) in an ultrasonic bath. After cleaning with distilled water, the etched aluminum alloy substrate was dried at 70 °C in a closed oven for more than 10 hr. The passivation process was performed by immersing the etched aluminum alloy substrate at room temperature in 0.01 M ethanolic SA solution for a range of passivation times. The morphological analyses of the samples were performed using a scanning electron microscope (SEM, JEOL JSM-6480 LV). The chemical composition of surfaces was analyzed by X-ray diffraction (XRD, D8 discover with Cu K_α wavelength 0.154 nm), Fourier Transform Infrared spectroscopy (FTIR, Perkins Elmer Spectrum One) and x-ray photoelectron spectroscopy (XPS, VG ESCALAB 220iXL) The XPS spectra were collected using an Al K_α (1486.6 eV) x-ray source. The wetting characterization of the sample surfaces was carried out by measuring static and dynamic contact angles using a First Ten Angstrom contact angle goniometer (the static contact angle has been abbreviated as CA and the dynamic contact angle has been abbreviated as contact angle hysteresis (CAH)). The adhesion of the superhydrophobic aluminum alloy substrates was carried out according to the ASTM D3359 standard test method using a Cross Hatch Cutter, model Elcometer

Accepted Manuscript

ACCEPTED MANUSCRIPT

107. The corrosion resistance properties of the samples were investigated via both potentiodynamic polarization experiments as well as electrochemical impedance spectroscopy (EIS). Electrochemical experiments were performed using a PGZ100 potentiostat and a 300 cm^3-EG&G PAR flat cell (London Scientific, London, ON, Canada), equipped with a standard three-electrode system with an Ag/AgCl reference electrode, a platinum (Pt) mesh as the counter electrode (CE), and the sample as the working electrode (WE) [6]. For the potentiodynamic polarization experiments, the open-circuit potential was scanned from -250 mV to +1000 mV in a 3.5 wt.% NaCl solution. An attempt was made to perform EIS measurements using 3 wt.% NaCl, as 3.5 wt.% was more reactive, in the frequency ranges between 0.01 Hz and 100 kHz with a sine-wave amplitude of 10 mV at room temperature.

3. Results and Discussion

3.1 Superhydrophobic aluminum alloy surfaces prepared by chemical etching followed by SA passivation

Figure 1(a) shows the SEM image of the surface of an as-received aluminum rolled sheet, which had a surface root-mean-square (rms) roughness of 0.45 μm and water contact angle (CA) of 87 ± 3° (inset of the Figure). The surface of rolled aluminum sheets generally exhibits the rolled lines and therefore will have a certain inherent roughness [32]. The CA of the SA passivated aluminum alloy substrate was found to be only 110 ± 1°. Therefore, a pretreatment of chemical etching using a 1 M alkaline NaOH solution was performed to modify the surface of the as-received aluminum alloy substrate. The morphology of the etched aluminum alloy substrate is shown in

Accepted Manuscript

ACCEPTED MANUSCRIPT

Figure 1(b). The NaOH etched aluminum alloy substrate (Figure 1(b)) was found to be rougher compared with the as-received aluminum alloy substrate (Figure 1(a)). Consequently, the surface roughness of the etched aluminum alloy substrate was increased to 1.38 ± 0.17 μm from 0.45 ± 0.03 μm of the as-received aluminum alloy substrate. The CA on the NaOH etched aluminum alloy substrate was decreased to 34 ± 4°, which can be attributed to the increase of surface area as well as the possible change of surface composition. The Wenzel model and its mathematical equation (Equation (1)) [33] can be used to explain the decrease of CA assuming no change of surface composition due to chemical etching.

$$\cos\theta^* = R_W \cos\theta \qquad \text{(Equation 1)}$$

where θ is the CA of a smooth surface and θ^* is the CA of a rough surface without any alteration of surface composition, the roughness factor R_w is the ratio of the true to the apparent surface areas. It is evident that R_w is always more than 1 as true surface area is larger than the apparent surface area due to the presence of roughness; therefore, as the CA of the as-received aluminum alloy substrate (assumed to be smooth) is 87 ± 3°, the CA of the etched rough surface would be smaller than 87 ± 3°. As the CA of the NaOH etched aluminum alloy substrate was 34 ± 4°, the R_w associated with the roughness of the etched substrate was calculated to be 15.84. However, it was not evident from the surface morphology that the surface area of the etched substrate could be 15 times more than that of as-received aluminum alloy. Therefore, the change of chemical composition due to the chemical etching process also played a role in the change of CA on the etched aluminum

Accepted Manuscript

ACCEPTED MANUSCRIPT

168 alloy substrate. We will see further that the SA passivation can modify the morphology of the NaOH
169 etched aluminum alloy substrate but is unable to modify the as-received aluminum alloy substrate,
170 which may due to the surface composition of the latter.
171

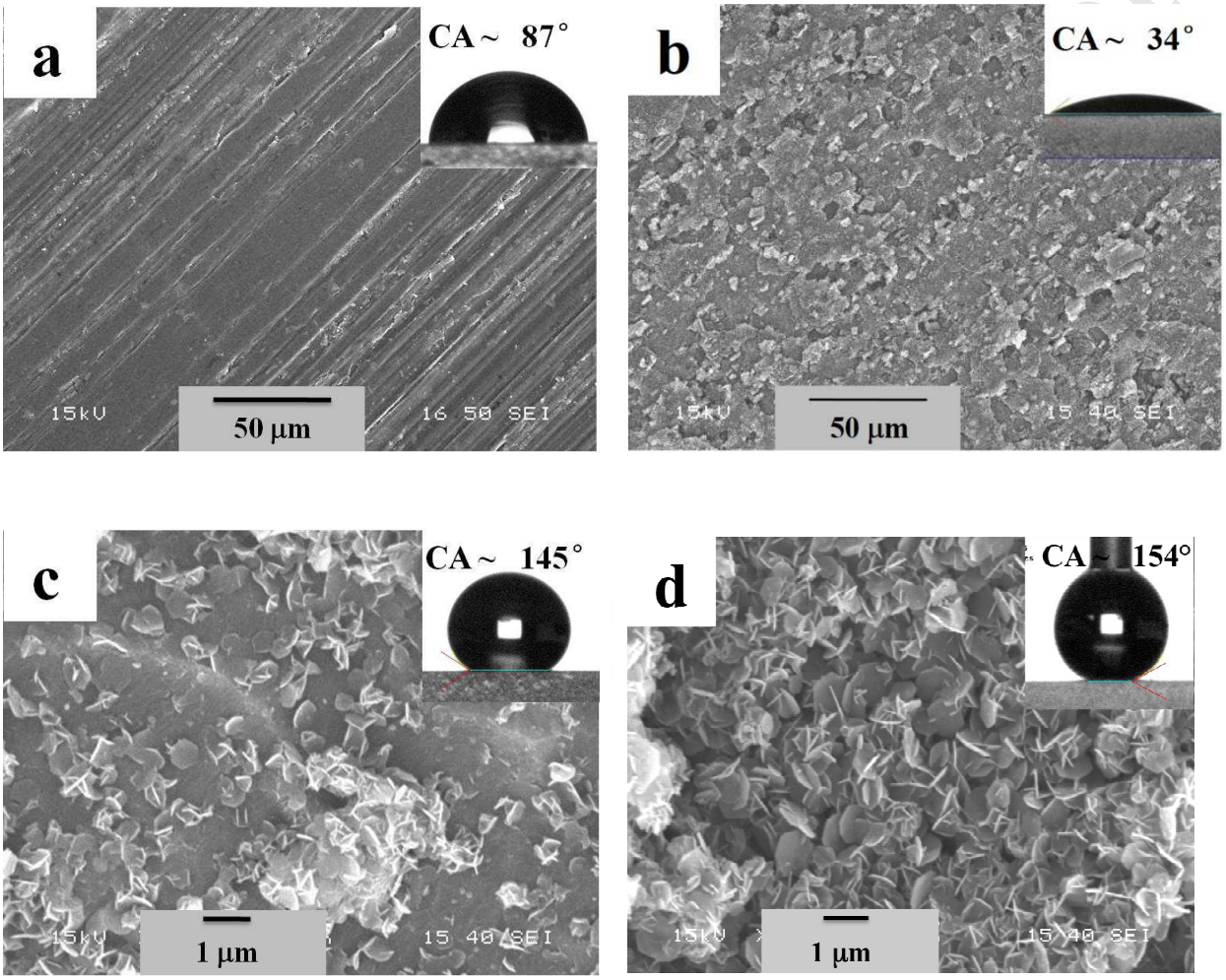

ACCEPTED MANUSCRIPT

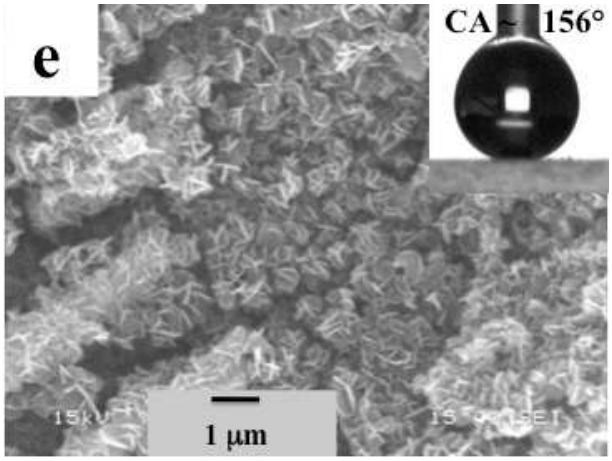

Figure 1 SEM images of the surface of (a) as-received aluminum alloy substrate; (b) NaOH etched aluminum alloy substrate; (c-e) 5 s-, 1 min- and 24 min-SA passivated NaOH etched aluminum alloy substrates. The insets of Figure 1(a-e) show the water drops and CA on the respective surfaces.

172

173 The NaOH etched aluminum alloy substrate was then passivated by SA for a range of
174 passivation times varying from couple of seconds to a maximum of an hour. Figure 1(c-e) shows the
175 morphologies of the NaOH etched aluminum alloy substrates followed by SA passivation for 5 s, 1
176 min and 24 min. The flake-like micro-nanostructure features appeared on the etched surface after
177 SA passivation for 5 s as shown in Figure 1(c). The inset of Figure 1(c) shows the image of a water
178 drop with a CA of 145 ± 2°. The enhancement of the CA was due to the formation of low surface
179 energy aluminum stearate (AlSA). The chemical analysis of these flake-like molecules is given in
180 Figure 2(a). The number density of these flake-like micro-nanostructures increased by increasing
181 the SA passivation time to 1 min, as shown in Figure 1(d). Consequently, the surface of etched
182 substrate is nearly covered with these flake-like structures just after 1 min of SA passivation. In this

ACCEPTED MANUSCRIPT

183 situation, the CA of this surface further increased to 154 ± 2°, as shown in the inset of Figure 1(d).
184 The compactness of these structures was further increased on the surface by increasing the SA
185 passivation time to 24 min, as shown in Figure 1(e). However, the CA did not increase much as
186 shown in the inset of Figure 1(e), yielding a value of 155 ± 1°. Because the surface morphology
187 from 60 min-SA passivation on etched aluminum alloy is very similar to that from 24 min-SA
188 passivation, the SEM image of that surface is not presented.
189

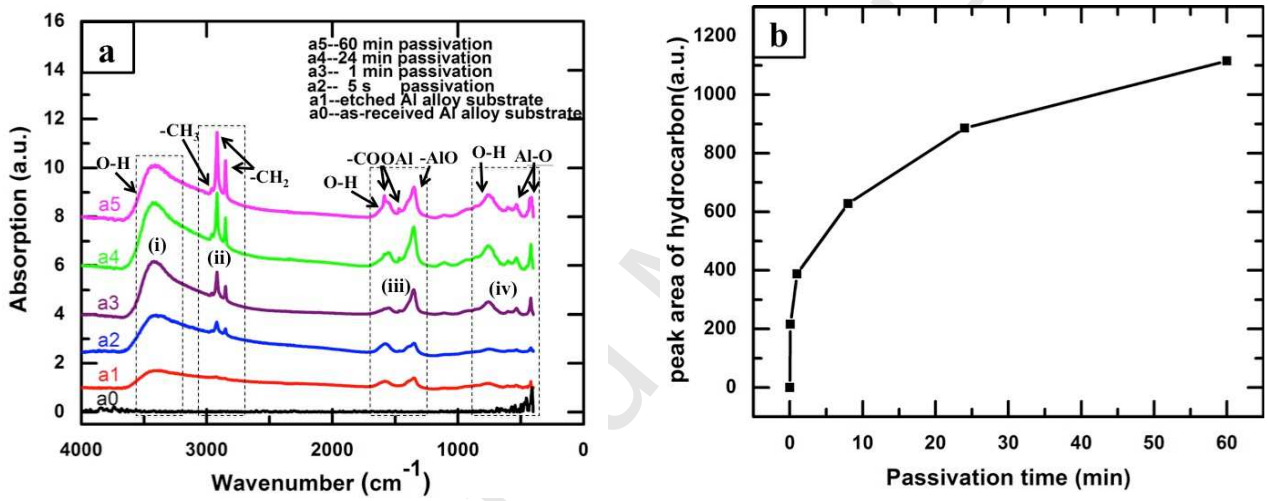

Figure 2(a) FTIR spectra of (a0) as-received aluminum alloy substrate, (a1) NaOH etched aluminum alloy substrate, and (a2) 5 s-, (a3) 1 min-, (a4) 24 min- and (a5) 60 min-SA passivated NaOH etched aluminum alloy substrates. Figure 2(b) depicts the variation in the area under the hydrocarbon (–CH_2 and -CH_3) peaks as a function of the SA passivation time.

190

191 The infrared spectra of the as-received aluminum alloy substrate, the NaOH etched aluminum
192 alloy substrate, and the SA passivated NaOH etched aluminum alloy substrates for a range of
193 passivation times are shown in Figure 2(a). The four main infrared absorption zones were observed
194 in all spectra. These zones are (i) a broad absorption peak between 3000-3500 cm^{-1}, (ii) two sharp

ACCEPTED MANUSCRIPT

absorption peaks at 2856 and 2917 cm^{-1}, (iii) an absorption zone approximately 1500 cm^{-1}, and (iv) a peak approximately 750 cm^{-1}. The broad absorption peak at 3420 cm^{-1} in zone (i) is assigned to -OH bonding on the NaOH etched aluminum alloy substrate, as shown in Figure 2(a1). As is evident in comparing with the spectrum of the as-received aluminum alloy substrate (Figure 2(a0)), the presence of –OH bonding at the surface of the NaOH etched aluminum alloy substrate may be due to possible –OH bond formation during the reaction of NaOH with the aluminum alloy substrate, as shown below using Equations (2-5):

$$2Al + 2NaOH + 6H_2O \rightarrow 2NaAl(OH)_4 + 3H_2 \quad \text{(Equation 2)}$$

(Equation 3)

$$Al_2O_3 + 2NaOH \rightarrow 2NaAlO_2 + H_2O \quad \text{(Equation 4)}$$

$$NaAlO_2 + H_2O \rightarrow Al(OH)_3 + NaOH \quad \text{(Equation 5)}$$

A similar reaction mechanism based on Equations 2 and 3 have been presented by Saleema *et al.* [6], who studied how to obtain superhydrophobic properties through a one-step process on aluminum alloy substrates using an alkaline NaOH solution containing FAS-17 molecules. However, they did not specify that the sodium aluminate ($NaAlO_2$) further hydrolyzed in the continuing reaction to produce $Al(OH)_3$ and NaOH. Furthermore, the presence of native oxides on aluminum alloy substrates most likely consists of aluminum oxide (Al_2O_3). Al_2O_3 on the surface of the aluminum alloy substrate can react with NaOH and form sodium aluminate ($NaAlO_2$), which can then hydrolyze to $Al(OH)_3$ and NaOH, as presented in Equation 4-5. Therefore, the above

Accepted Manuscript

ACCEPTED MANUSCRIPT

chemical reactions show that the aluminum alloy substrates will be covered with a layer of $Al(OH)_3$ after chemical etching with NaOH. Evidently, the appearance of the –OH peak in the IR spectrum (Figure 2(a1)) of the NaOH etched aluminum alloy substrate is in good agreement with the chemical reactions.

It was observed from the IR spectra of Figure 2(a) that the intensity of the –OH peak increased with the time of SA passivation. The formation of aluminum stearate (AlSA) ($CH_3(CH_2)_{16}COOAl(OH)_2$) (in Equation 6) as a reaction product between $Al(OH)_3$, present on the aluminum alloy substrates after NaOH etching, and SA was what led to the enhancement of the –OH peak after SA passivation (Figure 2(a2-a5)). The schematic illustration of the formation of AlSA on NaOH etched aluminum alloy substrates, engrafted with $Al(OH)_3$, is shown in Figure 3.

$$Al(OH)_3 + CH_3[(CH]_2)_{16}COOH \rightarrow CH_3[(CH]_2)_{16}COOAl(OH)_2 + H_2O \quad \text{(Equation 6)}$$

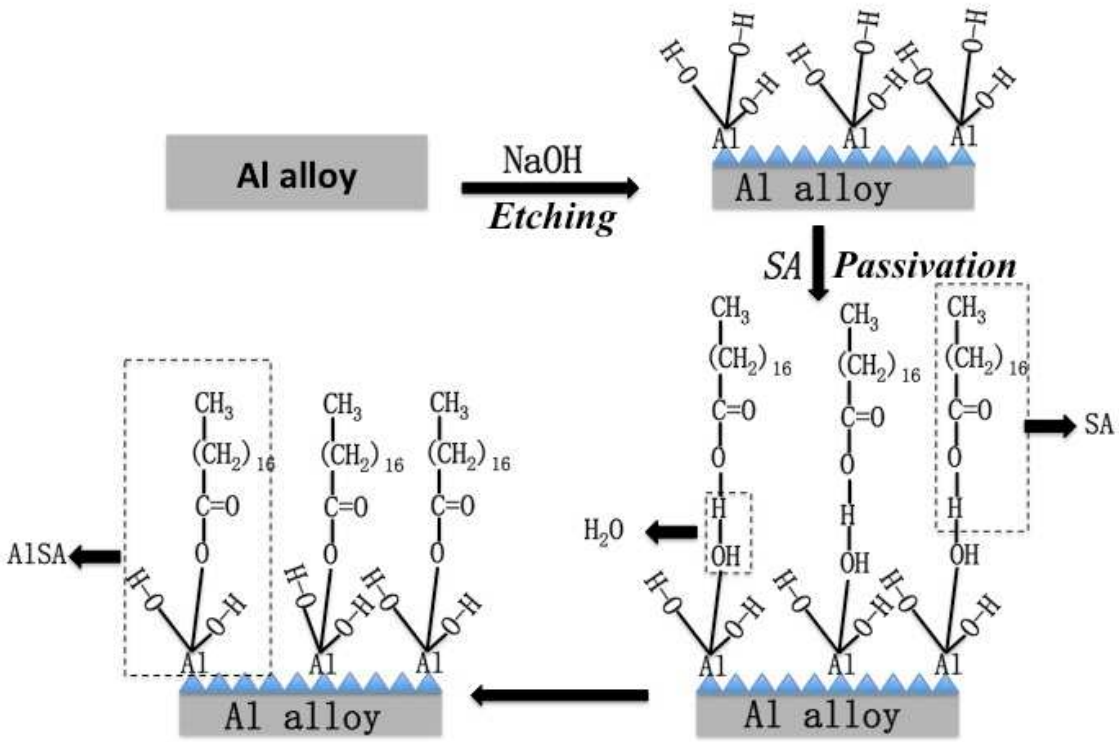

Figure 3 Schematic illustration of the formation of the superhydrophobic surface prepared by SA passivation on NaOH etched aluminum alloy substrate.

ACCEPTED MANUSCRIPT

It should be mentioned that, the appearance of –OH bonding on the NaOH etched aluminum alloy substrate is responsible for the formation of a superhydrophobic aluminum alloy substrate. However, the as-received aluminum alloy substrate without –OH bonding was unable to be passivated by SA solution, where it shows a maximum CA of 110 ± 1°

Furthermore, the peaks at 414, 536 and 607 cm^{-1} in zone (iv) may have appeared due to the Al-O bonding. The peaks at 1582 cm^{-1} in zone (iii) as well as 750 cm^{-1} in zone (iv) have also been assigned to the bending absorption mode of –OH, and the intensity of the peaks was also found to increase with the SA passivation time. The increasing intensity of the –OH peak as well as $–CH_2$ bonding with increasing passivation time indicate that greater AlSA formation took place, or, in other words, more amounts of SA molecules were adsorbed on the NaOH etched aluminum alloy substrates during the passivation process. Furthermore, in zone (iii), the infrared absorption peaks at 1586 and 1466 cm^{-1} were arising from –COOAl bonding; these peaks are more distinct on the IR spectrum of the samples passivated for 24 min (Figure 2(a5)). This is also in line with the analysis from SEM images (Figure 1(c-e)), where an increasing SA passivation time led to a thicker deposition of flake-like micro-nanostructures.

Compared with the –COOZn bonding at 1550 cm^{-1} presented in our recent publication on the superhydrophobic aluminum alloy substrate by SA-functionalized ZnO nanoparticles [32], the –COOAl bonding has shifted towards higher a wavenumber of 1586 cm^{-1} due to the lower atomic number of Al compared to that of Zn.

In addition, the two main sharp absorption peaks in zone (ii), which appeared at 2917 and 2851 cm^{-}

ACCEPTED MANUSCRIPT

248 [1], are ascribed to the asymmetric, symmetric C-H stretching modes, respectively, of $–CH_2$ groups on
249 the AlSA molecules. Additionally, a very small peak at 2956 cm^{-1} was present in the spectrum due
250 to the asymmetric in-plane C-H stretching mode of the $–CH_3$ group on the AlSA molecules.
251 The presences of absorption bands from –OH, –COOAl, $-CH_2$ as well as $–CH_3$ confirmed the
252 engrafting process of SA on NaOH etched aluminum alloy substrates, as modeled in Figure 3. The
253 model illustrates how hydrophilic components, such as –COO and –OH, bonding with the
254 aluminum alloy substrates kept the hydrophobic components, such as $–CH_2$ and $–CH_3$, away from
255 the surface, which effectively reduced the surface energy; hence, they are responsible for the
256 superhydrophobic properties. In our previous study, $-CH_2$, $-CH_3$ and –COO absorption peaks were
257 also observed in the spectrum of superhydrophobic copper surfaces fabricated by one-step
258 electrochemical modification [30]. It should be mentioned that unlike copper stearate (CuSA),
259 which does not have any –OH bonds [13], AlSA has two –OH bonds [34].
260 Because the intensity of the IR absorption peak of a molecule is proportional to its quantity, the
261 peak area of $–CH_2$ peak was monitored with the SA passivation time. It was observed that the
262 intensity of the $–CH_2$ peak of the passivated SA molecules increased with increasing SA passivation
263 time, as shown in Figure 2(a2-a5). Figure 2(b) depicts the variation of the peak areas of the $–CH_2$
264 and $–CH_3$ peaks as a function of the SA passivation time. Initially, a fast and almost linear increase
265 in the peak area was observed. The peak area was calculated to be 216 for the sample with 5 s-SA
266 passivation; the peak area increased to 388 for the sample with 1 min-passivation; the peak area
267 further increased to 886 for the sample with 24 min-SA passivation. Further increase of the peak
268 area to 1115 was also observed for the sample with 60 min-passivation. These observations are

Accepted Manuscript

ACCEPTED MANUSCRIPT

consistent with the morphological analysis by SEM, where an increase in the SA passivation time led to an increase in the density and thickness of AlSA flake-like micro-nanostructures.

Both XRD and XPS have been carried out to complement the observation of FTIR and validate the model on the formation of aluminum stearate. Figure 4 shows the low angle XRD between 2-12° and high angle XRD between 12-70° for both NaOH etched aluminum alloy substrate and SA passivated NaOH etched aluminum alloy substrates.

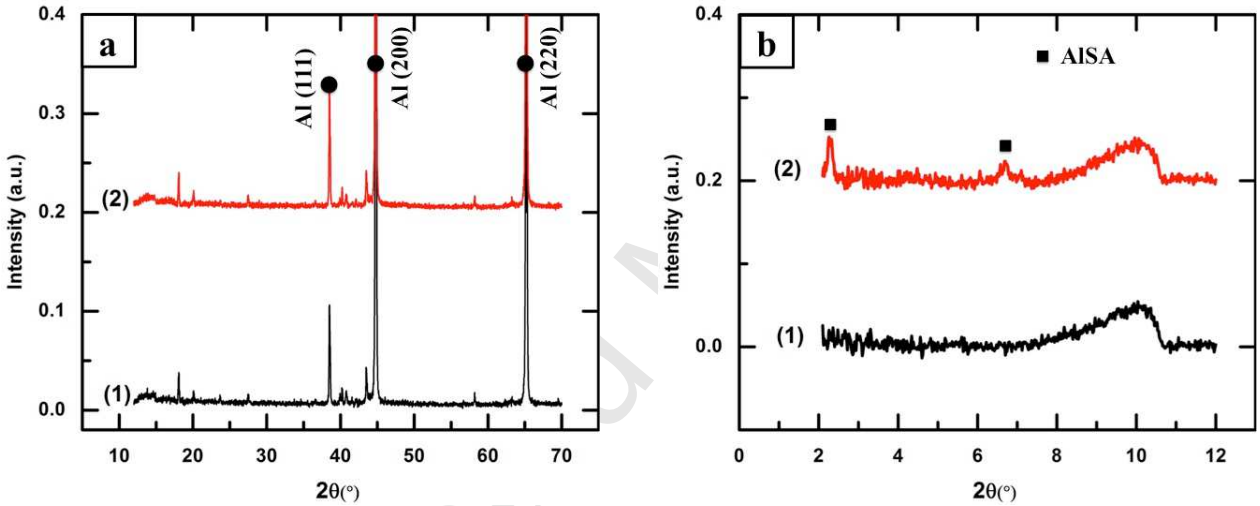

Figure 4 X-ray diffraction (XRD) patterns of (1) chemical etched aluminum alloy substrate and (2) stearic acid (SA) passivation on NaOH etched aluminum alloy substrate in the 2θ range of (a) 12-70° and (b) 2-12°. (Aluminum stearate is abbreviated as AlSA).

The X-ray diffraction (XRD) patterns of (1) chemical etched aluminum alloy substrate and (2) stearic acid (SA) passivation on NaOH etched aluminum alloy substrate are presented in Figure 4. As evident from the patterns at higher 2θ range of 12-70° in Figure 4(a), the characteristic peaks of Al (111), Al (200) and Al (220) at 38.47°, 44.72° and 65.1°, respectively, due to the aluminum alloy substrate [JCPDS # 01-085-1327]. Others small peaks are due to the intermetallic phases or the

ACCEPTED MANUSCRIPT

alloying elements. Figure 4 (b) shows the low angle XRD pattern between 2^{o} to 12^{o}. Figure 4(b2) shows two distinct diffraction peaks at 2.26° and 6.68° as compared to Figure 4(b1). These two peaks are due to the formation of aluminum stearate (AlSA). It is also complementary with the FTIR spectra of the SA-passivated NaOH etched aluminum alloy substrate, where the formation of aluminum stearate (AlSA) is discussed.

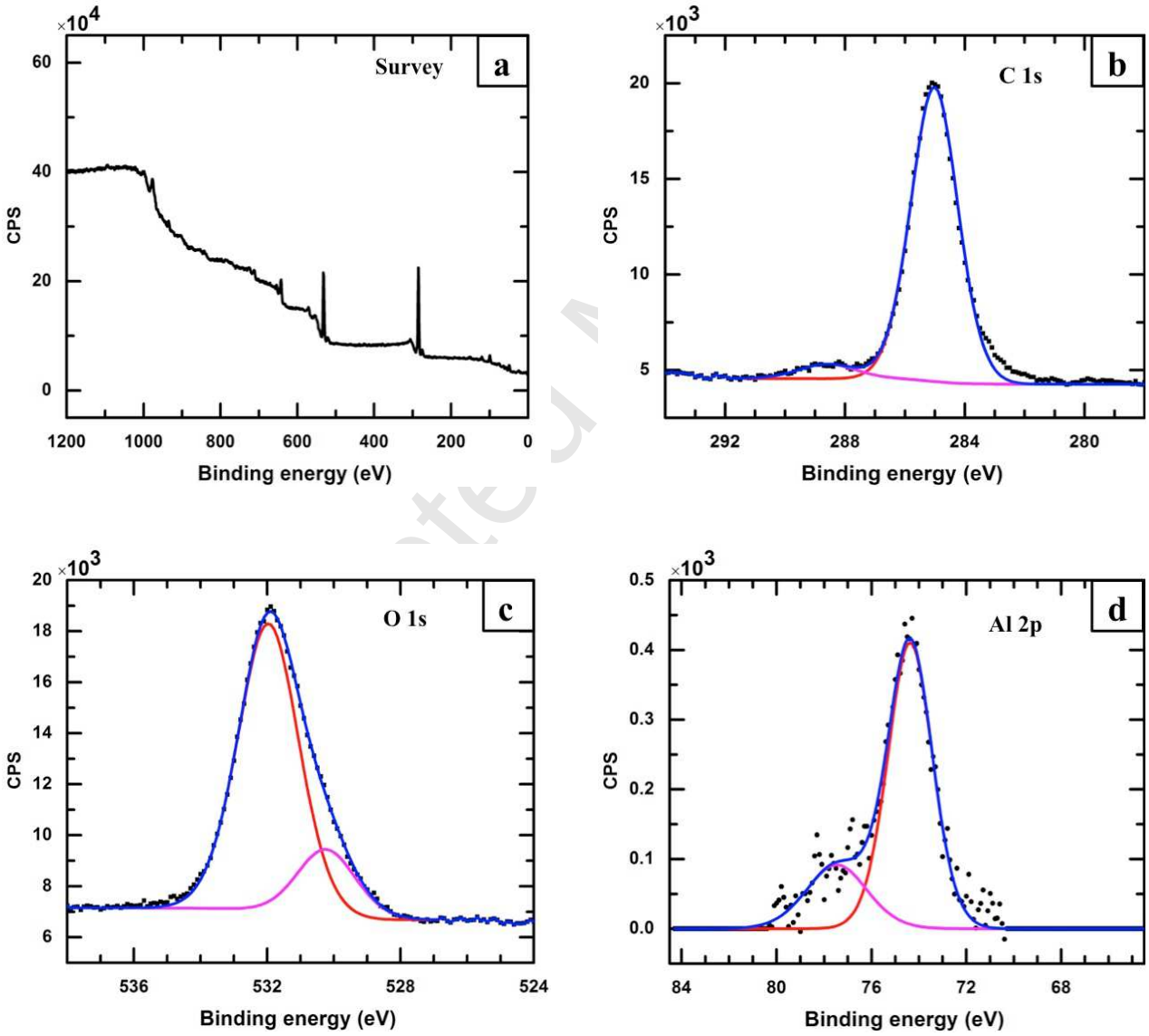

Figure 5 XPS spectra of the SA passivated NaOH etched aluminum alloy substrates (a) survey, (b) C 1s, (c) O 1s, (d) Al 2p

ACCEPTED MANUSCRIPT

Figure 5(a) shows the survey spectrum of the SA passivated NaOH etched aluminum alloy substrate. Two strong peaks of C 1s and O 1s are accompanied with a small peak of Al 2p. The Figure 5(b) shows the high resolution peak of C 1s that composed of a strong peak at 285 eV corresponds to C-C or C-H bonds and a tiny peak at 288.6 eV due to the –COO peak due to the formation of aluminum stearate. The ratio of the peaks area of –COO and C-C is found to be the 0.06 which is the finger print on the engrafting of stearic acid on a metal surface. Similar observations are reported on interaction of stearic acid with zinc [35, 36]. Figure 5(c) shows the O 1s peak that composed to two peaks having binding energy 530.2 eV and 531.9 eV corresponds to the bonding of Al-O and Al-OH, respectively [36]. Figure 5(d) shows the Al 2p that has two distinct peaks at 74.4 eV and 77.5 eV due to the bonding of Al-O and Al-OH, respectively [37]. The high resolution XPS peaks analysis on the C 1s, O 1s and Al 2p confirm the presence of –COO, C-H (or C-C) as well as Al-O and Al-OH as found by FTIR in Figure 2 and proposed in the model in Figure (3).

Figure 6(a-c) depict the variation of surface rms roughness, CA and CAH as a function of SA passivation time on the NaOH etched aluminum alloy substrates. The substrate has a surface rms roughness of 1.38 ± 0.17 μm and a CA of 34 ± 4°. The surface rms roughness and CA of the 5 s-SA passivated NaOH etched aluminum alloy substrate increased to 2.23 ± 0.18 μm and 145 ± 2°, respectively, due to the formation of flake-like micro-nanostructures of AlSA. The transition from a hydrophilic surface, i.e., the NaOH etched aluminum alloy substrate, to superhydrophobic surfaces

Accepted Manuscript

ACCEPTED MANUSCRIPT

occurred at the 1 min-SA passivation time mark, with a surface rms roughness of 2.29 ± 0.2 μm, a CA of 154 ± 2° and a CAH of 1.88 ± 0.4°. The appearance of surface superhydrophobicity was due to the formation of low surface energy AlSA, evident from the FTIR spectra, XRD patterns and XPS spectrum in Figure 2(a), Figure 4 and 5, respectively, as well as the presence of a micro-nanorough flake-like morphology, evident from the SEM images in Figure 1(d). The surface rms roughness remained constant from 1 min- to 24 min-SA passivation time but there was a slight tendency towards reduced roughness for SA passivation longer than 24 min. This reduction might be an indicator of the compactness of the passivated AlSA formation on the NaOH etched aluminum alloy substrates. On the other hand, the CA and CAH of the surfaces prepared by SA passivation were observed to remain constant with SA passivation times between 1 min to 60 min. The CA variation with SA passivation time has been reported in the literature [17, 38]. Ruan *et al.* prepared a superhydrophobic aluminum alloy substrate via chemical etching with HCl/HF solution followed by passivation with a different fatty acid. An optimum modified time of 1.5 h on the etched aluminum alloy substrate (with a CA of 167.6°) was observed by using lauric acid as the modifier, and the CA reduced to 155.2° for 2 h passivation [17]. The authors mentioned that the appearance of the optimum CA might have resulted from the change of surface morphology and microstructure due to different etching and modification parameters. However, the change of the surface morphology or the chemical composition with passivation time in their study was not investigated as performed here using SEM and FTIR, XRD as well as XPS. In the study by Kim *et al.*, a superhydrophobic substrate with a CA of 153° was produced by using a reactive ion etching process combined with hydrophobic coatings with PTFE [38]. The variation of the morphology

ACCEPTED MANUSCRIPT

330 with PTFE passivation time was found to contribute to the variation of the CA. However, the
331 chemical composition, one of the most important factors in superhydrophobicity, was not analyzed
332 in their study. In the literature, NaOH as an etchant has been utilized to prepare superhydrophobic
333 aluminum alloy substrates utilizing both one- and two-step processes [6, 21, 39].

334

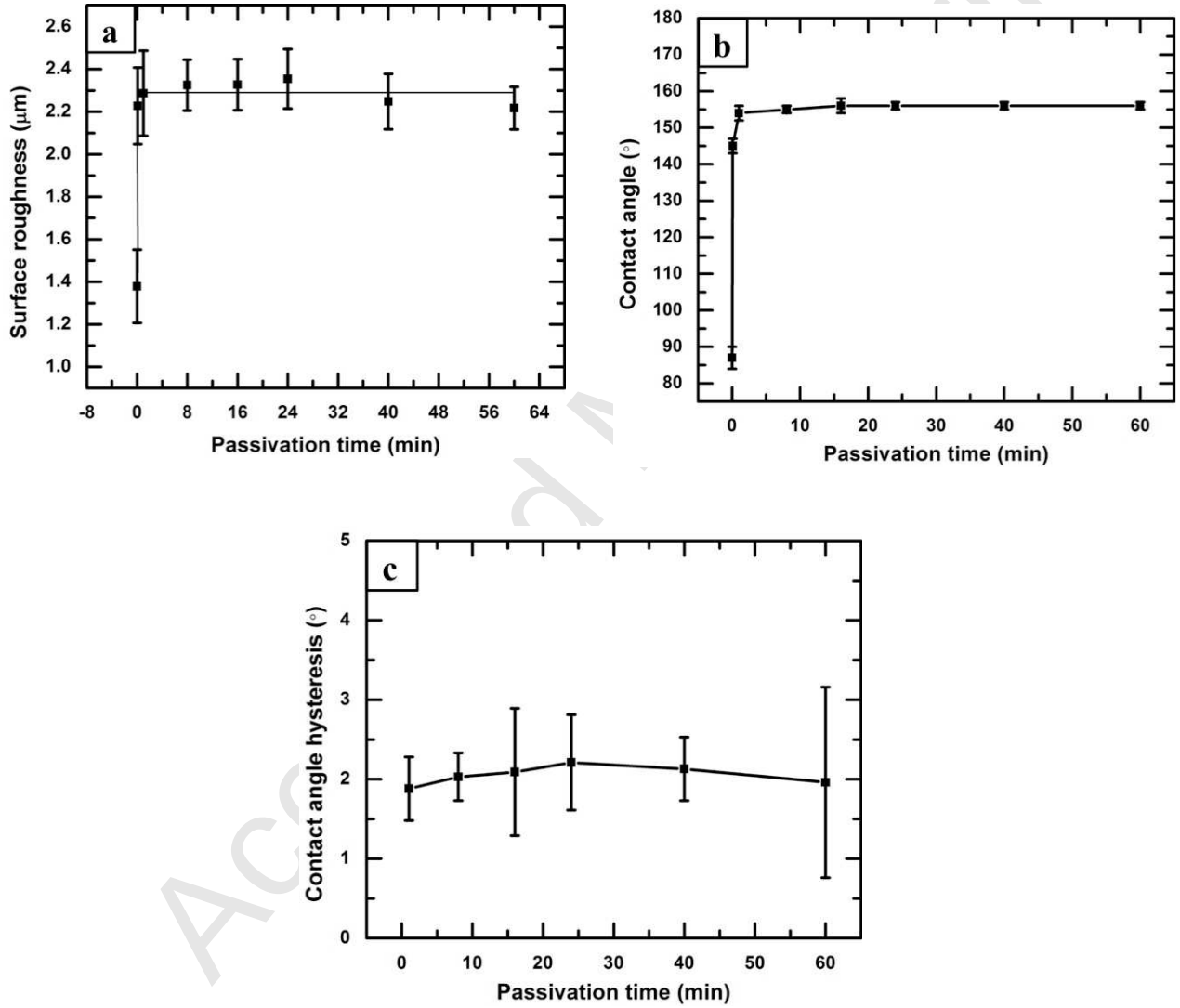

Figure 6(a) Surface root-mean-square (rms) roughness; (b) CA and (c) CAH variation as a function of SA passivation time on NaOH etched aluminum alloy substrates.

335

336 We have recently reported the formation of superhydrophobic aluminum alloys substrates,

ACCEPTED MANUSCRIPT

fabricated by electrodeposition of copper on aluminum alloy substrates followed by electrochemical modification using SA organic molecules, which provided similar CA [15]. Furthermore, Sarkar *et al.* (including one of the current authors) also studied superhydrophobic properties of ultrathin rf-sputtered Teflon films coated HCl etched aluminum alloy substrates [14]; the authors reported the effect of the etching time on the aluminum alloy substrates. A maximum CA of 164 ± 3° was observed on the ultrathin rf-sputtered Teflon coated aluminum substrates that were HCl etched for 2.5 min. Another study in our group fabricated superhydrophobic aluminum alloy substrates by monodispersive silica nanoparticles spin coating [40].

3.2 Corrosion resistance properties of superhydrophobic aluminum alloy substrates

Figure 7(a) shows the potentiodynamic polarization curves of the as-received aluminum alloy substrate, NaOH etched aluminum alloy substrate, and 5 s-, 1 min-, and 24 min-SA passivated NaOH etched aluminum alloy substrates. I_{corr} was calculated from the extrapolation of the cathodic curves [41]. R_p was calculated by the Stern-Geary equation, given by

$$R_p = \frac{\beta_a \beta_c}{2.3 I_{corr}(\beta_a + \beta_c)} \qquad \text{(Equation 7)}$$

where β_a and β_c are the anodic and cathodic Tafel slopes, respectively.

Accepted Manuscript

ACCEPTED MANUSCRIPT

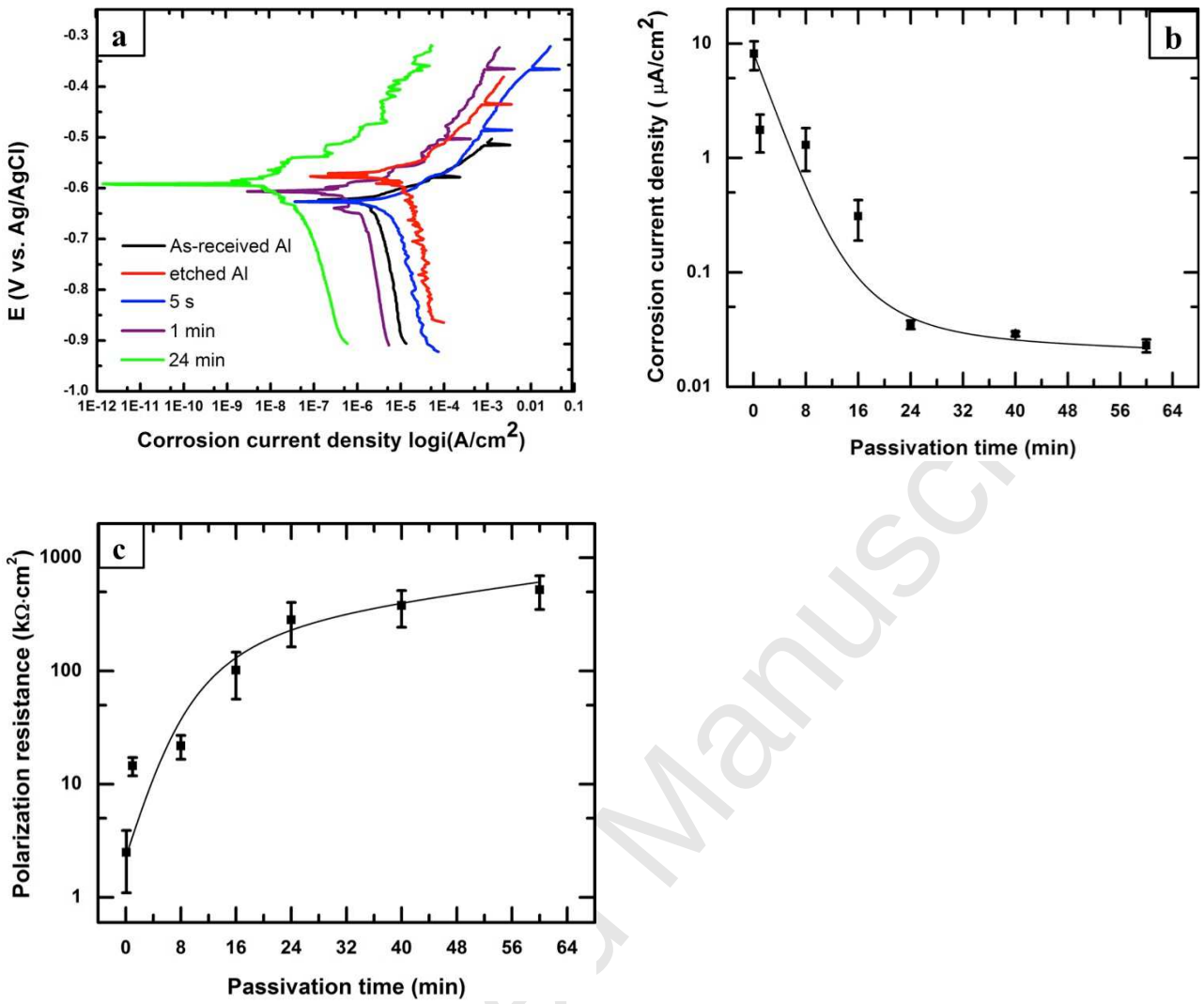

Figure 7(a) Potentiodynamic polarization curves of as-received aluminum alloy substrate, NaOH etched aluminum alloy substrate, and 5 s-, 1 min-, and 24 min-SA passivated etched aluminum alloy substrates. Variation of (b) I_{corr} and (c) R_p as a function of the SA passivation time on NaOH etched aluminum alloy substrates.

353

354 The I_{corr} and R_p of as-received aluminum alloy substrate were found to be 2.89 ± 0.8 μA/cm^2
355 and 3.79 kΩ·cm^2, respectively. The NaOH etched aluminum alloy substrate exhibited a larger I_{corr} of
356 16.29 ± 2.8 μA/cm^2 as well as a smaller R_p of only 2.24 kΩ·cm^2. This could be explained by the
357 increase of surface area as well as the loss of the protective oxide layer during the chemical etching

ACCEPTED MANUSCRIPT

process. This is consistent with the existing literatures, where it has been shown that the increase of surface roughness leads to similar trends in I_{corr} and R_p [42-44]. For example, in the study by Walter *et al.* [43], different surface roughness of AZ91 magnesium alloy, were obtained by polishing with different grits of silicon carbide (SiC) and 3 μm diamond paste, measured using atomic force microscopy (AFM). Consequently, it was observed that the I_{corr} of the AZ91 alloy in potentiodynamic polarization tests increased from 2.19 μA/cm^2 to 6.92 μA/cm^2 with an increase in the surface roughness from 0.08 μm to 0.43 μm.

Table 1 CA and CAH values and their respective I_{corr} and R_p values calculated by the Stern-Geary equation, as extracted from Figures 6 and 7 for SA passivation on NaOH etched aluminum alloy substrates for a range of passivation times.

Sample condition/SA passivation time	Contact angle CA (°)	Contact angle hysteresis CAH (°)	Corrosion current density I_{corr} (μA/cm^2)	Polarization resistance R_p (kΩ·cm^2)
As-received Al	87 ± 3	-	2.89 ± 0.8	3.79 ± 1.8
Etched Al	34 ± 4	-	16.29 ± 2.8	2.24 ± 0.98
5 s	145 ± 2	-	8.16 ± 2.3	2.50 ± 1.4
1 min	154 ± 2	1.88 ± 0.4	1.76 ± 0.64	14.53 ± 2.72
8 min	155 ± 1	2.03 ± 0.3	1.30 ± 0.53	21.83 ± 5.16

ACCEPTED MANUSCRIPT

16 min	156 ± 2	2.09 ± 0.8	0.31 ± 0.12	101.59 ± 45
24 min	156 ± 1	2.21 ± 0.6	0.035 ± 0.003	283.28 ± 120
60 min	156 ± 1	1.96 ± 1.2	0.023 ± 0.003	521.59 ± 171

In our case, the hydrophobic aluminum alloy substrate, prepared by 5 s-SA passivation on a NaOH etched aluminum alloy substrate, exhibited a lower value of I_{corr} of 8.16 ± 2.3 μA/cm^2 and a higher R_p of 2.5 kΩ·cm^2 compared with the aluminum alloy substrate treated with only NaOH etching, implying that the hydrophobic substrate inhibits corrosion of the substrate. However, these results are still inferior to that of the as-received aluminum alloy substrate, indicating that the hydrophobic surface having a water CA of 145 ± 2° is not resistant enough to prevent chemical attack from a corrosive environment.

However, both the anodic and cathodic current densities of superhydrophobic substrates, prepared with SA passivation longer than 1 min on NaOH etched alloy substrates, were significantly reduced, as observed in Figure 7(a). This reduction is due to a restricted supply of oxygen, as well as due to water-limiting oxygen and water reduction [45]. It is generally believed that the air trapped on the superhydrophobic surfaces behave as a dielectric for a parallel plate capacitor, which inhibits the electron transfer between the aluminum alloy substrate and the electrolyte and hence protects the substrate. The reduction in anodic current density of the superhydrophobic aluminum alloy substrates indicated that the anodic dissolution process was inhibited or postponed compared with the as-received aluminum alloy substrate [46]. Table 1 and Figure 7(b-c) show the variation of I_{corr} and R_p of the prepared samples. It should be mentioned that the 1 min-passivated NaOH etched aluminum alloy substrate, exhibiting a CA of 154 ± 2°, had a

Accepted Manuscript

ACCEPTED MANUSCRIPT

much lower I_{corr} of 1.76 ± 0.64 μA/cm^2 and a higher R_p of 14.53 kΩ·cm^2 compared with the as-received aluminum alloy substrate. With increasing SA passivation time up to 8 min and 16 min, I_{corr} values of the superhydrophobic aluminum alloy substrates reduced to 1.3 ± 0.53 μA/cm^2 and 0.31 ± 0.12 μA/cm^2, and R_p values increased to 21.83 kΩ·cm^2 and 101.59 kΩ·cm^2, respectively. The I_{corr} further decreased notably to 0.035 ± 0.003 μA/cm^2 and R_p increased to 283.28 kΩ·cm^2 for 24 min-SA passivation on NaOH etched aluminum alloy substrate. The R_p was found to increase as high as 521.59 kΩ·cm^2 after 60 min-SA passivation. It can be concluded that the I_{corr} value for the superhydrophobic aluminum alloy substrates were much lower than that of the as-received sample, and I_{corr} was found to decrease gradually with the increase of SA passivation time; on the other hand, the R_p values increased with the extended SA passivation time. Both the reduced I_{corr} and the enhanced R_p indicate that preparation by chemical etching followed by SA passivation process is effective for improving the corrosion resistance properties. It has been further shown that the corrosion inhibition of superhydrophobic surfaces by longer SA passivation times is superior to that of shorter passivation times.

It was observed that the corrosion potential (E_{corr}) increased as a function of the SA passivation time, from -0.627 V for 5 s-SA passivation to -0.578 V for 60 min-passivation on NaOH etched aluminum alloy substrates. This also suggests increasing corrosion resistance of the samples with extended passivation time. The more positive E_{corr} indicated that the surface could better prevent corrosion owing to the increasing density of AlSA molecules formed on the etched aluminum alloy substrates. Brassard *et al.* [31] has discussed the variation of E_{corr} on different Zn coated steel substrates followed by passivation with RTV-silicone and showed that superhydrophobic surfaces

Accepted Manuscript

ACCEPTED MANUSCRIPT

had higher E_{corr} compared to as-received aluminum alloy substrates. In our case, however, the E_{corr} increased with an increasing number density of AlSA molecules, that is, the E_{corr} still increased even when the CA remained constant on the superhydrophobic substrates prepared by different SA passivation times on the NaOH etched aluminum alloy substrates.

In the present study, another method was applied for calculating R_p, namely from the slope of the linear potential-current (E-I) curves by varying the potential ±10 mV around the corrosion potential (E_{corr}) and using Ohm's law (as shown in Figure 8(a))

$$R_p = \frac{\Delta E}{\Delta I} \quad \text{(Equation 8)}$$

where E and I are the potential and current, respectively.

The R_p calculated by Ohm's law (R_p1) values versus the R_p calculated by Stern-Geary equation (R_p2) values are plotted in Figure 8(b). As can be observed, there is excellent agreement between the R_p values calculated by the two methods. Furthermore, to evaluate the difference between R_p1 and R_p2, the relative error between them can be expressed as follows:

$$\text{Relative error} = \left|\frac{R_p2 - R_p1}{R_p2}\right| \times 100\% \quad \text{(Equation 9)}$$

According to the calculation, the relative error associated with corresponding R_p1 and R_p2 values is in the range of 10-20%, which indicates a good agreement between the R_p calculated by both Ohm's law and the Stern-Geary equation. The presence of small differences between the R_p values may be due to the differences in the Tafel slopes (β_a and β_c) and the slope of $\frac{\Delta E}{\Delta I}$ chosen in the analysis of the polarization curves. In this article (as well as in Table 1), the presented R_p was calculated using Stern-Geary equation (Equation 7).

The corrosion inhibition mechanism of superhydrophobic substrates by NaOH etching and SA

Accepted Manuscript

ACCEPTED MANUSCRIPT

passivation is similar to that in our previous study on the corrosion properties of superhydrophobic copper surfaces [30]. In that study, the superhydrophobic copper surfaces, fabricated by one-step electrochemical modification in an ethanolic SA solution, demonstrated improved corrosion resistance properties with increasing electrochemical modification time. In the present study, the corrosion properties of the etched and passivated substrates are significantly improved compared to the as-received substrate. The presence of the superhydrophobic AlSA flake-like morphology on the aluminum alloy substrate acted as a physical barrier to retard electrolyte penetration, as demonstrated by the gradual reduction of I_{corr} as well as enhanced R_p for longer SA passivation times. The corrosion test performed by Saleema *et al.* on a superhydrophobic aluminum alloy substrate prepared by a one-step process using a mixture of NaOH and FAS-17 solution did not provide any polarization data [6]; however, the superhydrophobic substrates formed corrosion pits after the polarization experiment. In the published literature, polarization curves have been widely used to analyze the corrosion resistance of superhydrophobic substrates; however, the R_p of superhydrophobic substrates compared with those of the as-received substrates were not presented in these studies [3, 47-49]. On the other hand, superhydrophobic coatings have been fabricated using myristic acid with cerium chloride solution on copper substrates [50]. In this study, polarization curves were presented to quantify the corrosion properties of Ce deposited superhydrophobic coatings, which had better corrosion resistance than the bare copper substrate. As the authors did not present the R_p of their coatings, we have used their values for β_a, β_c and I_{corr} to calculate the R_p of superhydrophobic Ce coatings in NaCl solution (3.5 wt.%) using the Stern-Geary equation (Equation 7): the calculated value of R_p was found to be 7.81 $k\Omega \cdot cm^2$. This calculated R_p

Accepted Manuscript

ACCEPTED MANUSCRIPT

452 value of for the Ce coated superhydrophobic copper substrate is much less than those for our
453 fabricated superhydrophobic substrates. Evidently, the R_p value of our superhydrophobic substrate
454 prepared by 60 min-SA passivation after NaOH etching is 66 times more than that of the
455 superhydrophobic copper substrate with Ce coating.

456

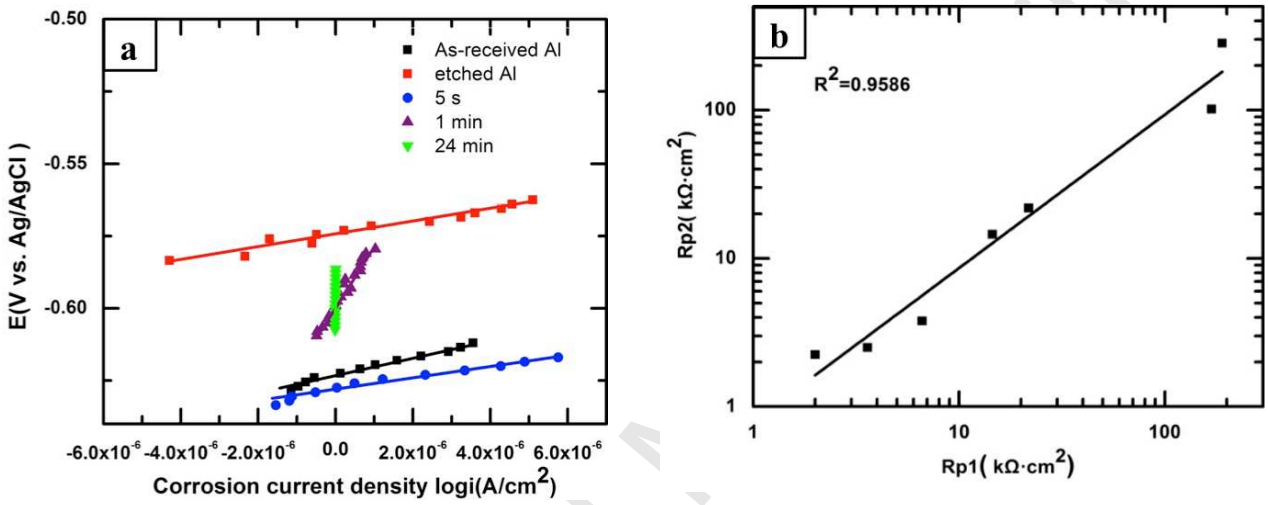

Figure 8(a) Potential-current (E-I) curves from varying the potential ±10 mV around the corrosion potential (Ecorr) for calculating Rp by Ohm's law; (b) Correlation between Rp calculated by (i) Ohm's law (Rp1) and (ii) the Stern-Geary equation (Rp2). R2 quantifies a measure of the goodness-of-fit of the linear regression.

457

458 Figure 9 shows the morphological and chemical composition changes of the hydrophobic substrates
459 prepared by 5 s-SA passivation and of superhydrophobic substrate that was prepared by 24 min-SA
460 passivation after corrosion tests. Compared with the image of the hydrophobic substrate before
461 corrosion testing, (Figure 9(a)), the SEM image of hydrophobic aluminum alloy substrate after
462 corrosion testing clearly indicates the formation of corrosion pits as marked by arrows in Figure
463 9(c); additionally, the CA was found to decrease from 145 ± 2° to 124 ± 6° after the corrosion test.

ACCEPTED MANUSCRIPT

464 The intensities of the $–CH_2$, $-CH_3$ and -COO peaks in the FTIR spectrum of the hydrophobic
465 substrate after corrosion were found to clearly decrease, as shown in the inset of Figure 9(e).
466 However, the surface morphology of superhydrophobic substrate remained the same before and
467 after the corrosion test, as shown in Figure 9(b, d)). Furthermore, no discernible variation in the
468 intensities of the $–CH_2$, $-CH_3$ and -COO peaks in the FTIR spectrum of the superhydrophobic
469 substrate were found before and after the corrosion test, as shown in Figure 9(f)). The inset images
470 of water drops also indicate the wetting properties remained the same. These results are consistent
471 with those from the polarization curves, which indicated that the superhydrophobic aluminum alloy
472 substrates had superior corrosion resistance as compared with both the as-received and hydrophobic
473 aluminum alloy substrates. As mentioned before, in the study by Saleema *et al.* on the corrosion
474 resistance property of superhydrophobic aluminum substrates prepared by chemical etching [6], a
475 poor corrosion resistance was observed in the superhydrophobic substrates, where a number of pits
476 formed after corrosion testing. Several other studies have also reported on the corrosion resistance
477 properties of superhydrophobic substrates [51-53]; however, until the current study, other works
478 have not reported on the variations in morphological, compositional and wetting properties of
479 superhydrophobic substrates.
480

Accepted Manuscript

ACCEPTED MANUSCRIPT

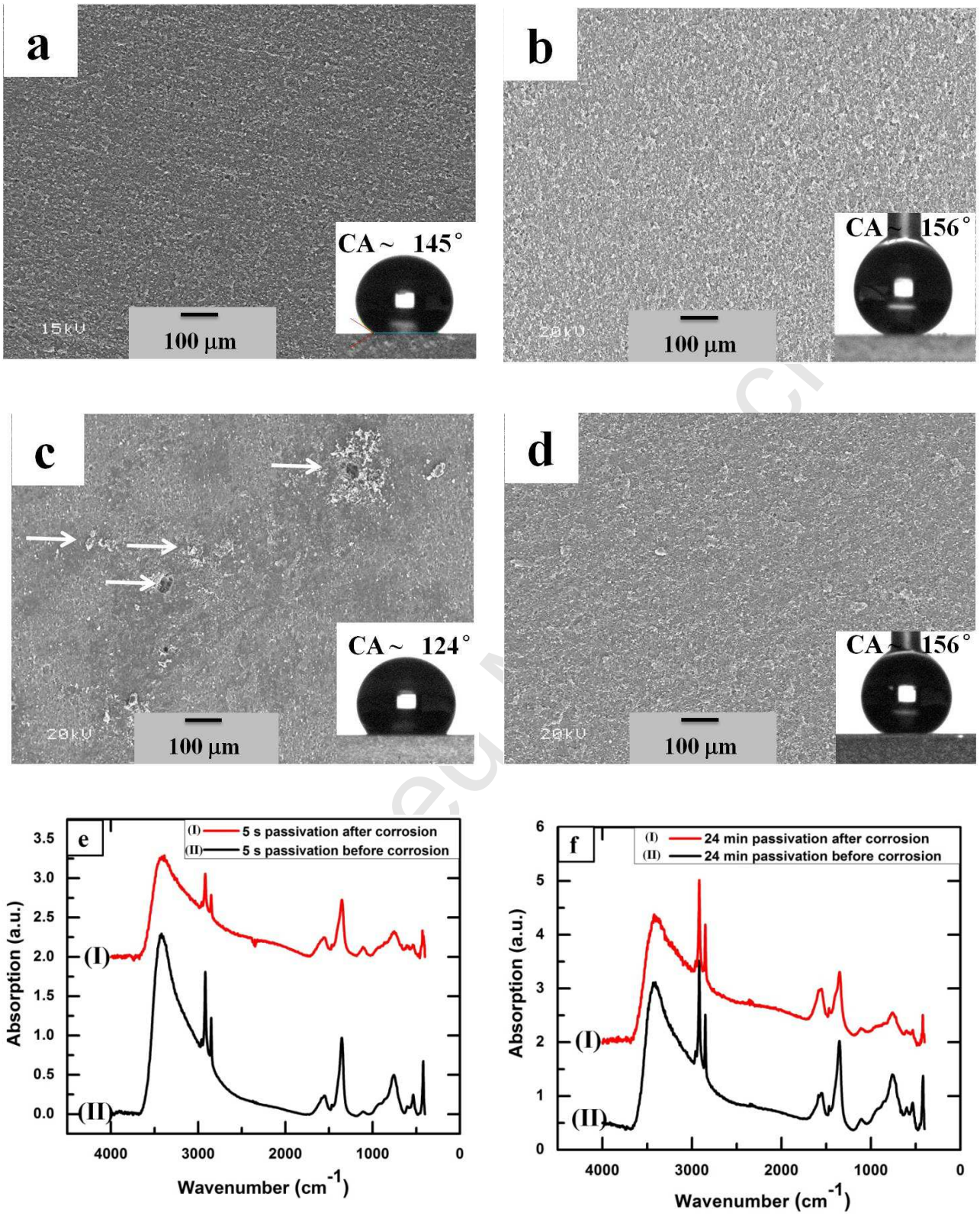

Figure 9 SEM images of the surfaces of the (a) 5 s- and (b) 24 min-passivated NaOH etched aluminum alloy substrates before corrosion, and (c-d) the surfaces after

ACCEPTED MANUSCRIPT

corrosion testing, respectively. The inset images show the water drops on the corresponding surfaces. Figure 9(e-f) shows FTIR spectra of the 5 s- and 24 min-passivated NaOH etched aluminum alloy substrates before (I) and after (II) corrosion, respectively.

481

482 An attempt has been made to evaluate the corrosion resistance of superhydrophobic surfaces using
483 electrochemical impedance spectroscopy (EIS) as a complementary tool to polarization resistance.
484 EIS was performed after immersing the samples in a salt solution for approximately 10 hr. The EIS
485 data have been analyzed in light of the analysis presented on the superhydrophobic surfaces
486 prepared on aluminum alloy substrates by Liu *et al.* [29] and Liang *et al.* [27]. Figure 10 shows the
487 Nyquist and Bode plots as well as the equivalent electrical circuits for the EIS data from the as-
488 received aluminum alloy substrate and the superhydrophobic aluminum alloy substrate prepared by
489 24 min-SA passivation. The graphs were plotted from the fitted data based on the equivalent
490 electrical circuit (see the supporting information for both original and fitted EIS plots). Specifically,
491 Figure 10(a) shows the Nyquist plots, which present the real component of impedance (Z_{real} or Z')
492 versus the imaginary component ($Z_{imaginary}$ or Z'') on a linear scale. Additionally, Figure 10 shows
493 the Bode plots, (b) modulus of impedance (|Z|) vs. frequency and (c) phase angle vs. frequency. The
494 diameter of the semicircle in the Nyquist plot signifies the charge transfer resistance (R_{ct}) of the
495 double layer formed at the interface between the sample surface and the corrosive medium. The
496 semicircle diameter of the Nyquist plot of the as-received aluminum alloy substrate was found to be
497 1.46 kΩ·cm^2 and is presented as an inset in Figure 10(a). On the other hand, two semicircles were
498 observed on the Nyquist plot of the superhydrophobic aluminum alloy substrate, as shown in Figure

Accepted Manuscript

ACCEPTED MANUSCRIPT

499 10(a). Among them, the smaller semicircle with a diameter of 29 kΩ·cm^2 at higher frequency (close
500 to the coordinate origin) represents the resistance of the superhydrophobic thin films (R_{SH}), and the
501 second large semicircle with a diameter of 95 kΩ·cm^2 represents charge transfer resistance (R_{ctSH})
502 of the double layer at the interface between the superhydrophobic surface and the salt solution. The
503 large value of impedance of the superhydrophobic film compared to the as-received aluminum alloy
504 surfaces shows that the superhydrophobic surfaces are more resistant against corrosion.
505

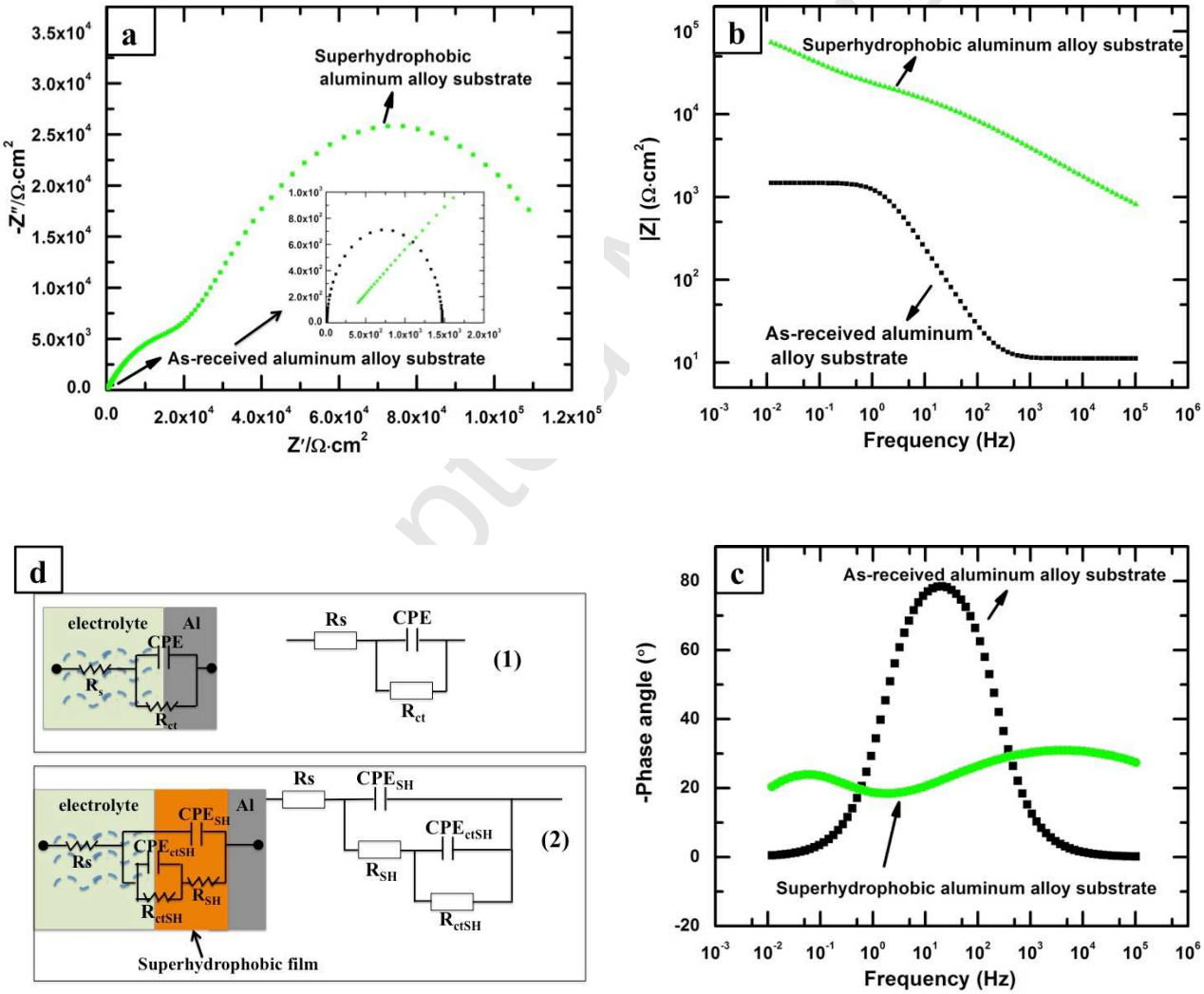

Figure 10(a) Nyquist plots, (b) Bode modulus diagrams and (c) Bode phase angle diagrams of as-received aluminum alloy substrate and superhydrophobic aluminum

ACCEPTED MANUSCRIPT

alloy substrate. (d) Electrical equivalent circuits for EIS of (d1) as-received aluminum alloy substrate and (d2) superhydrophobic aluminum alloy substrate. The insets image in (a) shows the enlargement of the high frequency region of the plots.

The top of Figure 10(b) shows the Bode plot of the superhydrophobic substrate, and bottom portion shows the Bode plot of the as-received aluminum alloy substrate. As observed in the bottom part of Figure 10(b), the as-received aluminum alloy substrate had a |Z| value of only 11.6 $\Omega \cdot cm^2$ at the high frequency of 10^4 Hz, in good agreement with the results presented by Liu *et al.* [29] and Liang *et al.* [27]. However, the superhydrophobic substrate exhibited a |Z| value of 1.74 $k\Omega \cdot cm^2$, which is nearly 150 times larger than that of the as-received aluminum alloy substrate at the same frequency. Similarly, at the low frequency of 0.01 Hz, the |Z| value of the as-received aluminum alloy substrate was found to be 1.06 $k\Omega \cdot cm^2$. In contrast, it was as high as 73.4 $k\Omega \cdot cm^2$ on the superhydrophobic aluminum alloy substrate. In general, AC impedance at high frequencies is the response of coatings with the solution and, at low frequency, reflects R_{ct} and the double-layer capacitance [54]. It is well known that the larger value of |Z| in the low frequency region signifies a better barrier in the thin film [52]. Therefore, according to the analysis of the Bode plots, the superhydrophobic substrate was found to have better corrosion resistance as compared with the as-received aluminum alloy substrate. It agrees well with the results from the polarization experiments, where R_p of the superhydrophobic surface was larger than that of the as-received aluminum alloy substrate, as shown in Table 1. This is comparable to the study by Liu *et al.* [29], where it was concluded, based on results from Bode plots, that the corrosion resistance of the graphene coated aluminum alloy was an order of magnitude higher than that of the uncoated aluminum alloy substrate. In the present

ACCEPTED MANUSCRIPT

study, compared with the as-received substrate, the corrosion resistance of the superhydrophobic aluminum alloy substrate was close to two orders of magnitude higher at low frequencies. This indicates that our superhydrophobic aluminum alloy substrate has better corrosion resistance than the graphene coated substrate [29]. This difference may be due to differences in the physical properties of graphene, in the case of Liu *et al.*, and aluminum stearate, in the current case.

Recently, Liang *et al.* fabricated silica-based superhydrophobic coatings on aluminum alloy substrates and performed EIS analysis [27]. In their work, the |Z| at 10 kHz of the superhydrophobic aluminum alloy substrate with a silica-based film, immersed for 30 minute in a salt solution, was reported to be 100 $\Omega \cdot cm^2$; the |Z| of the same sample was reported to be 2.5 $\Omega \cdot cm^2$ after increasing the immersion time to 24 hr. This reported |Z| value is even lower than those of their as-received aluminum alloy substrates. While comparing the impedance at 0.01 Hz, the |Z| value of the 30 min-immersed silica-based film coated superhydrophobic samples was reported to be 560 $k\Omega \cdot cm^2$, which further reduced to 16 $k\Omega \cdot cm^2$ after 8 hr of immersion. This value is very similar to that from our observations.

The Bode phase plot of the superhydrophobic substrate exhibits the two time constants, as shown in Figure 10(c). At the frequency of 25 Hz, the phase angle of the as-received aluminum alloy substrate arrived at the maximum value of 78°. However, the phase angle of the superhydrophobic surface exhibited the minimum value of 18.4° at a similar frequency. It is comparable with the study of Liu *et al.*, where two time constants were observed on the superhydrophobic aluminum alloy substrate fabricated by graphene spin coating [29]. The authors observed that the maximum phase angle value for the AA2024 aluminum alloy substrate was 75° and the lowest phase angle

Accepted Manuscript

ACCEPTED MANUSCRIPT

546 value of for the sample with the superhydrophobic graphene coating was 40° at the same frequency.
547 It is well known that phase angle (ϕ) is defined by the expression in Equation 10.
548

549 $$\varphi = arctan\left(\frac{|Z_{imaginary}|}{|Z_{real}|}\right)$$ (Equation 10)

550

551 Thus, a smaller phase angle indicates a larger value of Z_{real} (or Z'), which corresponds to a large
552 diameter in the Nyquist plot. In the current results from the Bode plots, the obtained phase angle of
553 18.4° for the superhydrophobic substrate is much smaller than that of 40° as reported by Liu et al.,
554 suggesting our superhydrophobic surface has better corrosion resistance than samples from the
555 latter.
556 Figure 10(d1) shows the equivalent electrical circuit of the as-received aluminum alloy surface in
557 reaction with the salt solution, as modeled by EIS. In this circuit, R_s is the resistance of the solution;
558 R_{ct} and CPE are the charge transfer resistance and the constant phase element associated with the
559 double layer formed at the interface between the aluminum surface and salt solution, respectively.
560 In the case of superhydrophobic coatings on the aluminum surface, an extra resistance R_{SH} and
561 constant phase element CPE_{SH} have been included in the circuit due to the dielectric nature of the
562 superhydrophobic coating. As the interaction of the salt with the superhydrophobic surface will be
563 different compared to that with untreated aluminum, the charge transfer resistance and constant
564 phase element associated with the double layer at the interface have been presented by R_{ctSH} and
565 CPE_{ctSH}. The assumption of this model is well supported by the observation of two time constants in
566 the Bode plot.

Accepted Manuscript

ACCEPTED MANUSCRIPT

Finally, the mechanical properties of the superhydrophobic substrate are very important for its uses against surface erosion, friction and corrosion [30]. The adhesion strength of all surfaces prepared by SA passivation after NaOH etching was found to be 5B, tested according to the ASTM D3359 standard.

4. Conclusions

Chemical etching of aluminum alloy substrates by NaOH followed by stearic acid (SA) passivation was used to prepare superhydrophobic aluminum alloy surfaces, and their corrosion resistance properties were investigated. The SA passivation process produces flake-like aluminum stearate micro-nanostructures on NaOH etched aluminum alloy substrates. The number density of these flake-like structures is observed to increase with the extension of SA passivation time. Investigations into the wetting properties of these surfaces demonstrated water contact angles of more than 150° after 1 min of SA passivation, which remained constant to 60 min of passivation time. However, the polarization resistance determined from polarization curves increases gradually from 3.79 to 521.59 $k\Omega \cdot cm^2$ for the as-received aluminum alloy substrates and the superhydrophobic surface prepared SA passivation for 60 min, respectively. Electrochemical impedance spectroscopy (EIS) shows that the moduli of impedance |Z| at lower frequencies for the as-received aluminum substrate and superhydrophobic aluminum substrate are 1.06 $k\Omega \cdot cm^2$ and 73.4 $k\Omega \cdot cm^2$, respectively. The higher values of the polarization resistance and modulus of impedance of the superhydrophobic aluminum surfaces with respect to the as-receive aluminum

Accepted Manuscript

ACCEPTED MANUSCRIPT

alloy surface demonstrate that the superhydrophobic surfaces prepared by chemical etching followed by SA passivation have superior corrosion resistance properties.

Acknowledgments:

We acknowledge the financial support provided by the Natural Science and Engineering Research Council of Canada (NSERC), Aluminum Research Center (REGAL) and Centre Québécois de Recherche et de Développement de l'aluminium (CQRDA).

References

(Primary Sources

Secondary Sources)

Uncategorized References

[1] C. Neinhuis, W. Barthlott, Characterization and Distribution of Water-repellent, Self-cleaning Plant Surfaces, Ann. Bot. 79 (1997) 667-677.
[2] J. Genzer, K. Efimenko, Recent developments in superhydrophobic surfaces and their relevance to marine fouling: a review, Biofouling, 22 (2006) 339-360.
[3] T. He, Y. Wang, Y. Zhang, Q. lv, T. Xu, T. Liu, Super-hydrophobic surface treatment as corrosion protection for aluminum in seawater, Corros. Sci. 51 (2009) 1757-1761.
[4] Y. Huang, D.K. Sarkar, X.G. Chen, Preparation of nanostructured superhydrophobic copper and aluminum surfaces, in, Adv. Mat. Res. 2012, pp. 497-501.
[5] J.D. Brassard, D.K. Sarkar, J. Perron, Synthesis of monodisperse fluorinated silica nanoparticles and their superhydrophobic thin films, ACS Appl. Mater. Interfaces 3 (2011) 3583.
[6] N. Saleema, D.K. Sarkar, D. Gallant, R.W. Paynter, X.G. Chen, Chemical Nature of Superhydrophobic Aluminum Alloy Surfaces Produced via a One-Step Process Using Fluoroalkyl-Silane in a Base Medium, ACS Appl. Mater. Interfaces 3 (2011) 4775-4781.
[7] N. Saleema, D.K. Sarkar, R.W. Paynter, X.G. Chen, Superhydrophobic Aluminum Alloy Surfaces by a Novel One-Step Process, ACS Appl. Mater. Interfaces 2 (2010) 2500-2502.
[8] S.D.K. Brassard J.D., Perron J., Fluorine Based Superhydrophobic Coatings, Appl. Sci., 2 (2012) 453-464.
[9] A. Safaee, D. Sarkar, M. Farzaneh, Superhydrophobic properties of silver-coated films on

ACCEPTED MANUSCRIPT

618 copper surface by galvanic exchange reaction, Appl. Surf. Sci. 254 (2008) 2493-2498.
619 [10] D.K. Sarkar, M. Farzaneh, R.W. Paynter, Wetting and superhydrophobic properties of PECVD
620 grown hydrocarbon and fluorinated-hydrocarbon coatings, Appl. Surf. Sci. 256 (2010) 3698-3701.
621 [11] D.K. Sarkar, M. Farzaneh, Superhydrophobic Coatings with Reduced Ice Adhesion, J. Adhes.
622 Sci. Technol. 23 (2009) 1215-1237.
623 [12] D.K. Sarkar, R.W. Paynter, One-Step Deposition Process to Obtain Nanostructured
624 Superhydrophobic Thin Films by Galvanic Exchange Reactions, J. Adhes. Sci. Technol. 24 (2010)
625 1181-1189.
626 [13] Y. Huang, D.K. Sarkar, X.G. Chen, A one-step process to engineer superhydrophobic copper
627 surfaces, Mater. Lett. 64 (2010) 2722-2724.
628 [14] D.K. Sarkar, M. Farzaneh, R.W. Paynter, Superhydrophobic properties of ultrathin rf-sputtered
629 Teflon films coated etched aluminum surfaces, Mater. Lett. 62 (2008) 1226-1229.
630 [15] Y. Huang, D.K. Sarkar, X.G. Chen, Fabrication of superhydrophobic surfaces on aluminum
631 alloy via electrodeposition of copper followed by electrochemical modification, Nano-micro lett.
632 3(3) (2011) 160-165.
633 [16] D.K. Sarkar, N. Saleema, One-step fabrication process of superhydrophobic green coatings,
634 Surf. Coat. Technol. 204 (2010) 2483-2486.
635 [17] M. Ruan, W. Li, B. Wang, Q. Luo, F. Ma, Z. Yu, Optimal conditions for the preparation of
636 superhydrophobic surfaces on al substrates using a simple etching approach, Appl. Surf. Sci. 258
637 (2012) 7031-7035.
638 [18] A.M. Escobar, N. Llorca-Isern, Superhydrophobic coating deposited directly on aluminum,
639 Appl. Surf. Sci. 305 (2014) 774-782.
640 [19] R. Liao, Z. Zuo, C. Guo, Y. Yuan, A. Zhuang, Fabrication of superhydrophobic surface on
641 aluminum by continuous chemical etching and its anti-icing property, Appl. Surf. Sci. 317 (2014)
642 701-709.
643 [20] Z. Zuo, R. Liao, C. Guo, Y. Yuan, X. Zhao, A. Zhuang, Y. Zhang, Fabrication and anti-icing
644 property of coral-like superhydrophobic aluminum surface, Appl. Surf. Sci. 331 (2015) 132-139.
645 [21] I. Bernagozzi, C. Antonini, F. Villa, M. Marengo, Fabricating superhydrophobic aluminum: An
646 optimized one-step wet synthesis using fluoroalkyl silane, Colloid. Surface *A.* 441 (2014) 919-924.
647 [22] Y. He, C. Jiang, H. Yin, J. Chen, W. Yuan, Superhydrophobic silicon surfaces with micro-nano
648 hierarchical structures via deep reactive ion etching and galvanic etching, J. Colloid Interface Sci.
649 364 (2011) 219-229.
650 [23] Y. Lu, W. Xu, J. Song, X. Liu, Y. Xing, J. Sun, Preparation of superhydrophobic titanium
651 surfaces via electrochemical etching and fluorosilane modification, Appl. Surf. Sci. 263 (2012) 297-
652 301.
653 [24] J. Sun, F. Zhang, J. Song, L. Wang, Q. Qu, Y. Lu, I. Parkin, Electrochemical fabrication of
654 superhydrophobic Zn surfaces, Appl. Surf. Sci. 315 (2014) 346-352.
655 [25] Y. Wang, W. Wang, L. Zhong, J. Wang, Q. Jiang, X. Guo, Super-hydrophobic surface on pure
656 magnesium substrate by wet chemical method, Appl. Surf. Sci. 256 (2010) 3837-3840.
657 [26] L. Pan, H. Dong, P. Bi, Facile preparation of superhydrophobic copper surface by HNO3
658 etching technique with the assistance of CTAB and ultrasonication, Appl. Surf. Sci. 257 (2010)
659 1707-1711.

ACCEPTED MANUSCRIPT

[27] J. Liang, Y. Hu, Y. Wu, H. Chen, Facile formation of superhydrophobic silica-based surface on aluminum substrate with tetraethylorthosilicate and vinyltriethoxysilane as co-precursor and its corrosion resistant performance in corrosive NaCl aqueous solution, Surf. Coat. Technol. 240 (2014) 145-153.

[28] T. Liu, L. Dong, T. Liu, Y. Yin, Investigations on reducing microbiologically-influenced corrosion of aluminum by using super-hydrophobic surfaces, Electrochim. Acta, 55 (2010) 5281-5285.

[29] Y. Liu, J. Zhang, S. Li, Y. Wang, Z. Han, L. Ren, Fabrication of a superhydrophobic graphene surface with excellent mechanical abrasion and corrosion resistance on an aluminum alloy substrate, RSC Adv. 4 (2014) 45389-45396.

[30] Y. Huang, D.K. Sarkar, D. Gallant, X.G. Chen, Corrosion resistance properties of superhydrophobic copper surfaces fabricated by one-step electrochemical modification process, Appl. Surf. Sci. 282 (2013) 689-694.

[31] J.D. Brassard, D.K. Sarkar, J. Perron, A. Audibert-Hayet, D. Melot, Nano-micro structured superhydrophobic zinc coating on steel for prevention of corrosion and ice adhesion, J. Colloid Interf. Sci. 447 (2015) 240-247.

[32] Y. Huang, D.K. Sarkar, X.G. Chen, Superhydrophobic nanostructured ZnO thin films on aluminum alloy substrates by electrophoretic deposition process, Appl. Surf. Sci. 327 (2015) 327-334.

[33] R.N. Wenzel, Resistance of solid surfaces to wetting by water, Ind. Eng. Chem. 28 (1936) 988-994.

[34] G. Osmond, J.J. Boon, L. Puskar, J. Drennan, Metal stearate distributions in modern artists' oil paints: Surface and cross-sectional investigation of reference paint films using conventional and synchrotron infrared microspectroscopy, Appl. Spectrosc. 66 (2012) 1136-1144.

[35] E. Johansson, L. Nyborg, XPS study of carboxylic acid layers on oxidized metals with reference to particulate materials, Surf. Interface Anal. 35 (2003) 375-381.

[36] A. Rittermeier, S. Miao, M.K. Schroter, X. Zhang, M.W.E. van den Berg, S. Kundu, Y. Wang, S. Schimpf, E. Loffler, R.A. Fischer, M. Muhler, The formation of colloidal copper nanoparticles stabilized by zinc stearate: one-pot single-step synthesis and characterization of the core-shell particles, Phys. Chem. Chem. Phys. 11 (2009) 8358-8366.

[37] C. Maldonado, J. De la Rosa, C. Lucio-Ortiz, A. Hernández-Ramírez, F. Barraza, J. Valente, Low Concentration Fe-Doped Alumina Catalysts Using Sol-Gel and Impregnation Methods: The Synthesis, Characterization and Catalytic Performance during the Combustion of Trichloroethylene, Materials 7 (2014) 2062-2086.

[38] B. Kim, S.-B. Seo, K. Bae, D.-Y. Kim, C.-H. Baek, H.-M. Kim, Stable superhydrophobic si surface produced by using reactive ion etching process combined with hydrophobic coatings, Surf. Coat. Technol. 232 (2013) 928-935.

[39] D. Xie, W. Li, A novel simple approach to preparation of superhydrophobic surfaces of aluminum alloys, Appl. Surf. Sci. 258 (2011) 1004-1007.

[40] J.-D. Brassard, D.K. Sarkar, J. Perron, Synthesis of Monodisperse Fluorinated Silica Nanoparticles and Their Superhydrophobic Thin Films, ACS Appl. Mater. Interfaces 3 (2011) 3583-3588.

ACCEPTED MANUSCRIPT

[41] D.G. Y. Han, X.-G. Chen, investigation on corrosion behavior of the Al-B4C metal matrix composite in a mildly oxidizing aqueous environment, Corrosion 67 (2011) 115005-115001.
[42] B. Yoo, K.R. Shin, D.Y. Hwang, D.H. Lee, D.H. Shin, Effect of surface roughness on leakage current and corrosion resistance of oxide layer on AZ91 Mg alloy prepared by plasma electrolytic oxidation, Appl. Surf. Sci. 256 (2010) 6667-6672.
[43] R. Walter, M.B. Kannan, Influence of surface roughness on the corrosion behaviour of magnesium alloy, Mater. Design 32 (2011) 2350-2354.
[44] A. Shahryari, W. Kamal, S. Omanovic, The effect of surface roughness on the efficiency of the cyclic potentiodynamic passivation (CPP) method in the improvement of general and pitting corrosion resistance of 316LVM stainless steel, Mater. Lett. 62 (2008) 3906-3909.
[45] H. Liu, S. Szunerits, W. Xu, R. Boukherroub, Preparation of superhydrophobic coatings on zinc as effective corrosion barriers, ACS Appl. Mater. Interfaces 1 (2009) 1150-1153.
[46] W. Xiao, R. Man, C. Miao, T. Peng, Study on corrosion resistance of the BTESPT silane cooperating with rare earth cerium on the surface of aluminum-tube, J. Rare Earths 28 (2010) 117-122.
[47] Y. Cheng, S. Lu, W. Xu, H. Wen, Fabrication of Au-AlAu4-Al2O3 superhydrophobic surface and its corrosion resistance, RSC Adv. 5 (2015) 15387-15394.
[48] Y. Fan, Z. Chen, J. Liang, Y. Wang, H. Chen, Preparation of superhydrophobic films on copper substrate for corrosion protection, Surf. Coat. Technol. 244 (2014) 1-8.
[49] Q. Liu, Z. Kang, One-step electrodeposition process to fabricate superhydrophobic surface with improved anticorrosion property on magnesium alloy, Mater. Lett. 137 (2014) 210-213.
[50] C. Liu, F. Su, J. Liang, P. Huang, Facile fabrication of superhydrophobic cerium coating with micro-nano flower-like structure and excellent corrosion resistance, Surf. Coat Technol. 258 (2014) 580-586.
[51] P. Wang, D. Zhang, R. Qiu, B. Hou, Super-hydrophobic film prepared on zinc as corrosion barrier, Corros. Sci. 53 (2011) 2080-2086.
[52] F. Zhang, S. Chen, L. Dong, Y. Lei, T. Liu, Y. Yin, Preparation of superhydrophobic films on titanium as effective corrosion barriers, Appl. Surf. Sci. 257 (2011) 2587-2591.
[53] B. Yin, L. Fang, A.-q. Tang, Q.-l. Huang, J. Hu, J.-h. Mao, G. Bai, H. Bai, Novel strategy in increasing stability and corrosion resistance for super-hydrophobic coating on aluminum alloy surfaces, Appl. Surf. Sci. 258 (2011) 580-585.
[54] G.X. Shen, Y.C. Chen, L. Lin, C.J. Lin, D. Scantlebury, Study on a hydrophobic nano-TiO2 coating and its properties for corrosion protection of metals, Electrochim. Acta 50 (2005) 5083-5089.